Spin glass in the bond-diluted J_1-J_2 Ising model on the square lattice

Yining Xu and Dao-Xin Yao*

State Key Laboratory of Optoelectronic Material and Technologies, School of Physics, Sun Yat-sen University, Guangzhou 510275, China

(Received 29 December 2017; published 18 June 2018)

We use Monte Carlo (MC) methods to simulate a two-dimensional (2D) bond-diluted Ising model on the square lattice, which has frustration between nearest-neighbor interaction J_1 and next-nearest-neighbor interaction J_2. In this study, we use the parallel tempering algorithm to study thermodynamics for different diluted ratios x [where $x = N(J_2)_{\text{diluted}}/2N$, where N denotes the system volume] and present a phase diagram. The presence of frustration and disorder results in a spin-glass phase, which exists between the stripe antiferromagnetic phase and Néel phase. We present a ground-state energy of $T \to 0$ and the size dependence of the Edwards-Anderson (EA) order parameter for the spin-glass phase. By scaling the mean energy and EA order parameter from the simulated annealing with the Kibble-Zurek mechanism, we obtain two different dynamic exponents, z_E and z_q, for the spin-glass phase. Experimentally, this model has a close relationship with the FeAs plane of the iron-based superconductor $BaFe_2(As_{1-x}P_x)_2$, where a spin-glass-like phase was found.

DOI: 10.1103/PhysRevB.97.224419

I. INTRODUCTION

Considerable theoretical and experimental efforts have been dedicated to studying the properties of a spin glass [1], in which spins are frozen and disordered. A theoretical model of spin glasses was proposed by Edwards and Anderson [2]. Spin-glass models, such as the Edwards-Anderson model and Sherrington-Kirkpatrick model [3], were originally studied by mean-field theory. Initially, replica symmetry breaking was not considered in spin glasses until the Almeida-Thouless line [4] was discovered. In experiment, several of the characteristic phenomena, such as the rather sharp cusp in the frequency-dependent susceptibility in low fields [5] and remanence [6,7] and hysteresis below the freezing temperature [8,9], have been observed in spin glass. The behavior of spin glass can be observed through methods such as nuclear magnetic resonance (NMR) and neutron scattering (NS). Among the spin-glass systems, the two-dimensional (2D) Ising spin glass (ISG) is a special kind because these systems exist only at temperature $T = 0$ [10]. The commonly discussed 2D ISG models, such as the square lattice with Gaussian or bimodal couplings, contain randomly distributed ferromagnetic and antiferromagnetic interactions. In recent years, numerous studies [11–15] have focused on low-temperature behavior and phase transition in the 2D ISG.

In addition to the frustrated interactions, disorder, such as dilutions, plays an important role in spin glass. Bond dilution can be realized by changing the interactions between two spins. Site dilution can be achieved by removing or changing a certain portion of the spins on the lattice. Numerous investigations [16–19] have been conducted to locate the transition point and critical behavior by using renormalization-group and Monte Carlo (MC) methods. Diluted spin models can be realized in many materials. For example, $Fe_xZn_{1-x}F_2$ and $Mn_xZn_{1-x}F_2$ are prepared by substituting nonmagnetic isomorph ZnF_2 into the magnetic $FeF_2(MnF_2)$ and can be described as a three-dimensional diluted Ising model [20]. The modulation of a pairing symmetry with bond dilution in iron-based superconductors was studied in Ref. [21]. In the present study, we study a 2D bond-diluted Ising model with the nearest-neighbor interaction J_1 and next-nearest-neighbor interaction J_2 on the square lattice, which is similar to the FeAs plane of the iron-based superconductor $BaFe_2(As_{1-x}P_x)_2$. The spin size of the Fe atoms is generally large, and the magnetic transitions in undoped $BaFe_2As_2$ are found to be in the 2D Ising universality class [22,23]. Therefore, we use Ising spins to describe magnetism. The random distribution of P atoms can lead to an effective J_2 dilution on the square lattice. A spin-glass-like behavior in $BaFe_2(As_{1-x}P_x)_2$ [24] was found by NMR and triple-axis spectrometer (TRISP) measurements, where the superconductivity also occurs [25,26]. However, a systematic study on magnetism was lacking.

Fundamentally, understanding the thermodynamics of the 2D bond-diluted J_1-J_2 Ising model, which is different from the clean J_1-J_2 Ising model [27–30], is also interesting. Our study confirms that the system has a spin-glass phase, which can be controlled by bond dilution and frustration.

In this study, we use the highly efficient MC methods (i.e., parallel tempering and simulated annealing) to study the 2D bond-diluted J_1-J_2 Ising model. We investigate the thermodynamics of the ordered phase as the dilution ratio x. A spin-glass phase is found between the stripe antiferromagnetic phase and Néel phase. In the spin-glass phase, we find two different dynamic exponents, which are obtained from the simulated annealing results of the mean energy and Edwards-Anderson (EA) order parameter. This unusual behavior is similar to the results of the 2D $\pm J$ ISG model in Ref. [15]. The phase diagram can help in understanding the experimental phase diagram of $BaFe_2(As_{1-x}P_x)_2$.

The rest of this paper is organized as follows. In Sec. II we introduce the model and methods. Numerical results are

*Corresponding author: yaodaox@mail.sysu.edu.cn

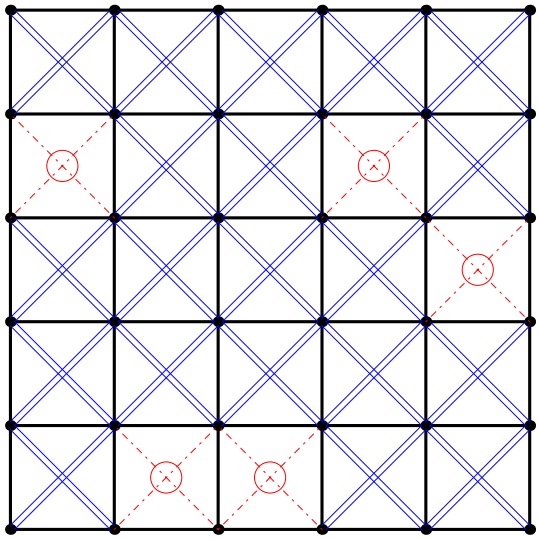

FIG. 1. Two-dimensional square-lattice Ising model with two types of interaction. The thick solid line represents the nearest-neighbor interaction J_1. The blue double line indicates the next-nearest-neighbor interaction J_2. J_2 constantly comes in pairs in a plaquette and can be broken in pairs (i.e., bond dilution), as denoted by the red dashed lines.

presented in Sec. III, including the spin-glass phase and its dynamic properties. In Sec. IV we discuss a comparison of our results and the experimental results. Conclusions are given in Sec. V. The Appendix provides additional results, which discuss the connections with the 2D $\pm J$ ISG model.

II. MODEL AND METHODS

A. Model

We study a bond-diluted J_1-J_2 Ising model on the 2D square lattice, as illustrated in Fig. 1. The structure of this model is similar to the FeAs plane of the iron-based superconductor $BaFe_2(As_{1-x}P_x)_2$. The Hamiltonian of the model is as follows:

$$H = J_1 \sum_{\langle i,j\rangle} \sigma_i \sigma_j + J_2 \sum_{\langle i',j'\rangle} \delta_{i'j'} \sigma_{i'} \sigma_{j'}, \quad \sigma_i = \pm 1, \qquad (1)$$

where J_1 is the nearest-neighbor interaction, J_2 denotes the next-nearest-neighbor interaction, and $\delta_{i'j'}$ represents the bond dilution (1 indicates the existence of a J_2 bond; 0 refers to the bond dilution, as depicted in Fig. 1). J_2 constantly comes in pairs in a plaquette and can be broken in pairs. We define the bond dilution ratio as $x = N(J_2)_{\text{diluted}}/2N$, where N is the system volume. Here, we set $J_1 = J_2 = 1$.

In $BaFe_2(As_{1-x}P_x)_2$, magnetism and superconductivity occur in the FeAs plane, where the As atoms sit alternatively above and below the center of each plaquette on the square lattice which is formed by the Fe atoms, as demonstrated in Fig. 2. In the FeAs plane, the P atoms can be randomly substituted for the As atoms.

In our study, we consider the spin magnetism of the Fe atoms. The spins on the Fe atoms are regarded as Ising spins because the spin size of the Fe atoms is generally large, and the magnetic transitions in undoped $BaFe_2As_2$ are found to be in the 2D Ising universality class [22,23]. The nearest-neighbor

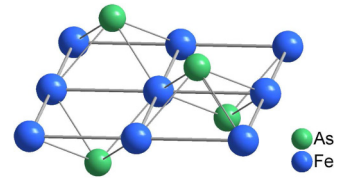

FIG. 2. FeAs plane of $BaFe_2(As_{1-x}P_x)_2$. Fe atoms form a square lattice. Here, x is the doping ratio of $BaFe_2(As_{1-x}P_x)_2$. Parts of the As atoms are substituted by the P atoms when $x > 0$.

interaction between the Fe atoms is defined as J_1. The As atoms generate the superexchange interactions between the Fe atoms, while the P atoms cannot. An As atom constructs a pair of J_2 among four Fe atoms. J_2 is broken in pairs when the As atom is substituted for the P atom. x is the doping ratio of the P atoms and equals the diluted ratio that we defined.

In this model, a competitive relationship occurs when J_1 and J_2 exist simultaneously because these interactions are antiferromagnetic and form a triangular structure. Our random dilution results in a disordered distribution of J_2, similar to the disordered doping in the $BaFe_2(As_{1-x}P_x)_2$ material. The competitive interactions cause frustration, and the disorder is introduced into the system by random dilution. Our study obtains an interesting discovery considering the combination of frustration and disorder.

B. Parallel tempering

For complex systems, the energy landscape has numerous separated local minima. The simulation of complex systems through the conventional MC method typically requires an extensive relaxation time. In conventional MC studies, simulations of high temperatures are generally sampled in large volumes of phase space, whereas the low-temperature ones may be trapped in the local energy minima during the timescale of a typical computer simulation. To solve this problem, several MC methods, such as parallel tempering [31], population annealing [32], and simulated annealing [33], have been discussed. The form of parallel tempering MC, which is frequently used, dates back to Geyer [34]. In the developmental process, parallel tempering has many similar forms, such as replica Monte Carlo [35], simulated tempering [36], and the expanded ensemble method [37]. All of these methods simulate complex systems over a wide temperature range, thereby helping complex systems to escape from metastable states and speeding up the equilibrium process.

The parallel tempering method used here allows the system to exchange the complete configuration among different temperatures, thus ensuring that the low-temperature system can access a set of representative regions of phase space. We briefly summarize the sampling procedure of the parallel tempering method. The operation is implemented in two stages, namely, the simple single-temperature MC stage and parallel tempering stage. In the simple MC stage, N noninteracting replicas of the system are simulated simultaneously by performing a single-temperature Metropolis update at N temperatures, e.g., $T_1, T_2, \ldots, T_N$. The parallel tempering stage conducts replica exchange, where two replicas at neighboring temperatures swap the complete configuration. The swapping probability

p_{swap} between two neighboring temperatures, T_i and T_{i+1}, is defined by

$$p_{\text{swap}} = \min\left\{1, \exp\left[\left(\frac{1}{T_{i+1}} - \frac{1}{T_i}\right)(E_{i+1} - E_i)\right]\right\}, \quad (2)$$

where E_i and E_{i+1} are the energies of the replica at temperatures T_i and T_{i+1}, respectively.

Currently, the parallel tempering MC is widely regarded as a powerful method for studying complex systems. In this study, we aim to use the improved form, which adjusts the steps of the two stages or the distribution of the temperatures [38–40], for example, mainly adjusting the temperature distribution around the critical value to increase the effective data volume. These improvements can make the computation more efficient.

C. Simulated annealing

The method is called simulated annealing because it is similar to physical annealing [41]. In physical annealing, a crystal is heated and then cooled slowly until achieving common crystal lattice structures so that the defects of the crystal can be removed. If cooling is sufficiently slow, then the final configuration can approach a superior structure. Numerically, simulated annealing establishes the connection between the thermodynamic behavior of physical annealing and the search for the global minima of a discrete optimization problem [33,42].

For spin systems with a rough energy landscape, simulated annealing is a sequential MC process. In the beginning, finding the equilibrium state at the initial temperature by using the standard Metropolis update is necessary. Then, the temperature is slowly decreased to the critical temperature, with updating the system in the temperature of every step. Simulated annealing is a powerful algorithm for exploring the energy landscape of complex systems and is capable of escaping from the local minima. Simulated annealing and parallel tempering play a similar role in detecting the ground states of complex systems [43], but their differences are distinct. Simulated annealing is a nonequilibrium process, which does not provide any meaningful results during the annealing process except for the nonequilibrium results obtained from the critical temperature. The nonequilibrium results acquired after the annealing process are related to the annealing velocity and system size. The study of phase transitions with simulated annealing is based on the Kibble-Zurek (KZ) mechanism [44,45], which was originally used in the nonequilibrium scaling of the defect density in condensed-matter physics and is successfully used at present to describe nonequilibrium physics at classical and quantum phase transitions.

III. NUMERICAL RESULTS

A. Ordered phase

From the Hamiltonian, we can easily find that the ground state of the system is the Néel state when the dilution ratio $x = 1$, which implies that the system has no J_2 interaction. The antiferromagnetic interactions J_1 and J_2 exist simultaneously when the dilution ratio $x = 0$, thereby introducing frustration into the system. However, the J_1 and J_2 bonds are distributed in an ordered pattern; thus, the ground state of the system exhibits the stripe antiferromagnetic order. In this section, we focus on the change in the ground state as a function of x. Under different dilutions, we investigate the critical temperature of the transition from ordered phases to the paramagnetic phase. We use an order parameter m_s [28] to describe the stripe antiferromagnetic order, which can be defined as

$$\begin{aligned} m_s^2 &= m_x^2 + m_y^2, \\ m_x^2 &= \frac{1}{N}\sum_{i=1}^{N} \sigma_i (-1)^{x_i}, \\ m_y^2 &= \frac{1}{N}\sum_{i=1}^{N} \sigma_i (-1)^{y_i}. \end{aligned} \quad (3)$$

The Néel order parameter is calculated as

$$m_N = \frac{1}{N}\sum_{i=1}^{N} \sigma_i (-1)^{x_i + y_i}. \quad (4)$$

To locate the critical temperatures, we define the Binder cumulant [46] as

$$B_m = \frac{\langle m^4 \rangle}{\langle m^2 \rangle^2}, \quad (5)$$

where m represents m_s or m_N. Specific heat C is also computed to study the phase transition from an ordered state to the paramagnetic state. We exhibit the results of $x = 0.1$ in Fig. 3 and perform the same analysis for the rest of x. For the same dilution of x, the disorder distribution can be reset before each simulation considering the influence of disorder on the system. We average over thousands of independent disordered distributions to determine the converged values of these physical quantities.

We obtain the critical temperatures $T_c(L)$ from the crossing points of the curves for L and $2L$. We obtain the critical temperature T_c for the thermodynamic limit by performing the power-law fitting. In Fig. 4, we present an instance with $x = 0.1$.

We can obtain a series of critical points when changing the dilution ratio x. In Fig. 5(a), the critical temperature of the system decreases continuously to zero, where the long-range order disappears, with the increase in disorder. We can see that the stripe antiferromagnetic phase has $x_c = 0.31(1)$ and the Néel phase has $x_c = 0.73(2)$ by sweeping the whole range of x in [0,1]. The phase diagram obtained here can help us to understand the experimental phase diagram of $BaFe_2(As_{1-x}P_x)_2$, as discussed in Sec. IV.

B. Spin-glass phase

We study the spin-glass phase, which appears in the intermediate region of x ($0.31 < x < 0.73$). The EA order parameter q [2] is defined as

$$q = \frac{1}{N}\sum_{i=1}^{N} \sigma_i^{(1)} \sigma_i^{(2)}, \quad (6)$$

which measures the autocorrelation of spin σ_i between the two replicas. In Ref. [2], the spin glass should have the characteristics of the magnetization $|m| = 0$ and EA order

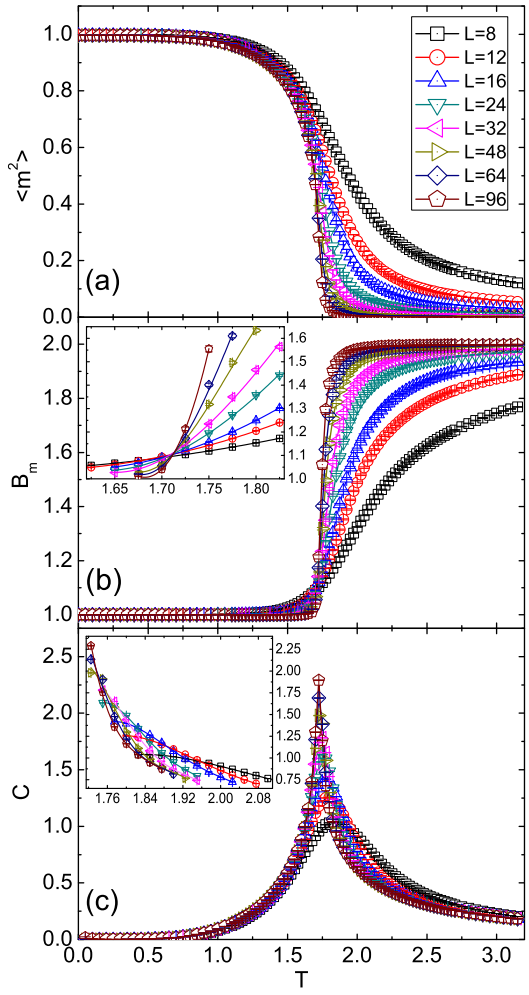

FIG. 3. Results of $x = 0.1$, where the dilution of the system is insufficient to change the order of the ground state. (a) Order parameter indicates that the ground state has a stripe antiferromagnetic order. The results of the Binder cumulant are presented in (b), and (c) corresponds to the specific heat. We obtain the crossing points, which correspond to the critical temperature $T_c(L)$, by polynomial fitting to the data.

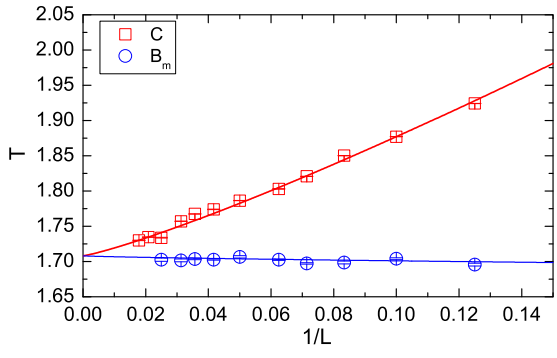

FIG. 4. $T_c(L)$ obtained from the specific heat C and Binder cumulant B_m. The system has long-range order when $x = 0.1$. We can extrapolate $T_c(L)$ to an infinite size and finally obtain the corresponding critical temperature $T_c(\infty)$ of x by using the form $T_c(L) = T_c(\infty) + a/L^b$. Here, a and b are the fitting parameters, and the critical temperature $T_c(\infty) = 1.708(9)$.

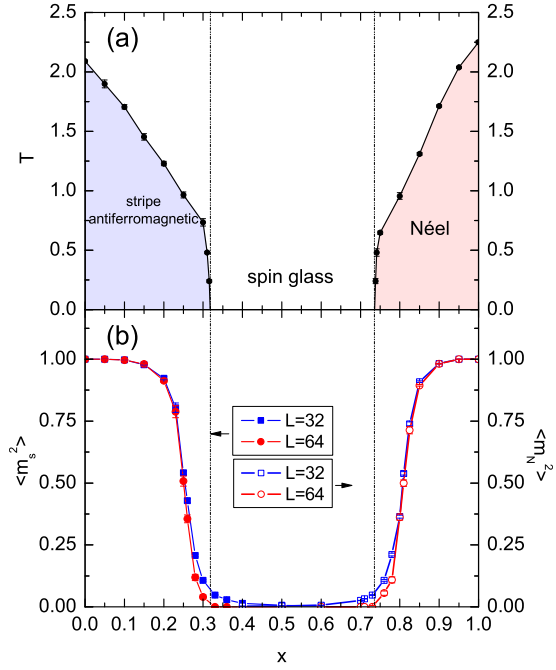

FIG. 5. (a) The phase diagram. We obtain two smooth phase boundaries by computing the critical temperature through a series dilution ratio x. The system is in the stripe antiferromagnetic phase or the Néel phase below the critical temperatures, whereas the upper region is the paramagnetic phase. The critical temperature gradually decreases when x changes from the two sides to the middle until the critical point cannot be measured given the disappearance of the long-range order. The x_c at $T = 0$ is obtained by extrapolating from the neighboring points because we cannot find the x_c value of $T = 0$ through classical MC. Here, x_c of the stripe antiferromagnetic phase is 0.31(1), and x_c of the Néel phase is 0.73(2). (b) Results of order parameters m_s^2 and m_N^2. $T = 0.00003$ is used. The solid points indicate the results of m_s^2, and the open points correspond to m_N^2.

parameter $|q| > 0$. The magnetization here is m_s or m_N, which is used as the order parameter of the ordered phase. Figure 5(b) illustrates the results of m_s and m_N. Section III B 1 describes the results of the EA order parameter and presents the existence of the spin-glass phase.

1. Equilibrium finite-size scaling

Here, we discuss the differences among the 2D ISG models. From the perspective of the energy landscape, the 2D ISG model with Gaussian coupling has a nondegenerate ground state, thereby implying the EA order parameter $|q|_{T=0} = 1$, whereas the 2D $\pm J$ ISG model has infinitely degenerate ground states. From this perspective, our model is similar to the 2D $\pm J$ ISG model, in which $|q|$ can be expressed as a function of size when $T = 0$ [15].

As mentioned previously, the 2D ISG exists only at $T = 0$; thus, achieving the exact zero-temperature results is difficult for classical MC simulations. However, the 2D ISG properties can still be obtained by considering the weak dependence of the EA order parameter on temperature when $T \to 0$, as depicted in Fig. 6(a).

The EA order parameter is an important criterion for defining and describing the spin glass. Here, we show the $\langle q^2 \rangle$

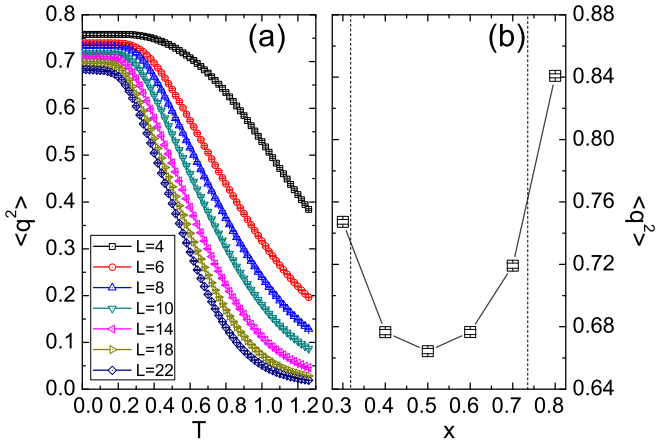

FIG. 6. (a) The equilibrium $\langle q^2 \rangle$ of different system sizes vs T when $x = 0.5$. In the region of $T \to 0$, $\langle q^2 \rangle$ has a weak temperature dependence, and the values continue to decrease with the increase in size. (b) Results of $\langle q^2 \rangle$ vs x; we use the dashed lines to mark the spin-glass region. The minimum value appears at $x = 0.5$. $L = 24$ and $T = 0.00002$ are used.

values within the spin-glass region in Fig. 6(b). We use the fixed value $x = 0.5$ as a sample in the following discussion because the minimum of $\langle q^2 \rangle$ appears at $x = 0.5$, which represents the most disordered state of the model.

We use the finite-size scaling relation [15] $A(T,L) = L^{-\kappa\Theta_s} f(TL^{\Theta_s})$, where Θ_s is the entropy exponent. The value of Θ_s in the 2D $\pm J$ ISG model [47] is obtained by scaling the spin-glass correlation function. We obtain the same result $\Theta_s \cong 0.5$ by performing the same scaling used by Ref. [47] in our model demonstrated in the Appendix. Therefore, we include a finite-size correction term [15] to find the value of $\langle q_{\rm eq}^2 \rangle$ in the thermodynamic limit as follows:

$$\langle q_{\rm eq}^2(L) \rangle - \langle q_{\rm eq}^2(\infty) \rangle \propto L^{-\Theta_s}. \tag{7}$$

In Ref. [48], the ground-state energy of the spin glass is expressed by the finite-size correction, which is eventually written as $E(L)_0 - E(\infty)_0 \propto L^{-(d+1/\nu)}$. The ν of the case that we studied here is discussed in the Appendix. Thus, we obtain $\nu \to \infty$, thereby leading to the correction of the ground-state energy being written as

$$\langle E_0(L) \rangle - \langle E_0(\infty) \rangle \propto L^{-2} \qquad (d = 2). \tag{8}$$

From the correction of the EA order parameter and the ground-state energy, we obtain the size-dependent relationship and the thermodynamic limit of $\langle q_{\rm eq}^2(L) \rangle$ and $\langle E_0(L) \rangle$ as displayed in Fig. 7. Here, we obtain $\langle q_{\rm eq}^2(\infty) \rangle = 0.649(4)$ and $\langle E_0(\infty) \rangle = -1.4279(2)$. In accordance with the characteristic of the spin glass, which is $|m| = 0$ and $|q| > 0$, we can confirm that the spin-glass phase exists between the two ordered phases because the value of $\langle q_{\rm eq}^2(\infty) \rangle$ is greater than zero.

For $x = 0.4$ and 0.65, the same calculations are performed by using Eqs. (7) and (8) with the same exponents Θ_s and ν. The exponents here have universality in the spin-glass phase.

2. Kibble-Zurek scaling

In the calculations, numerous updates are required to approach the equilibrium state, especially as $T \to 0$. Therefore,

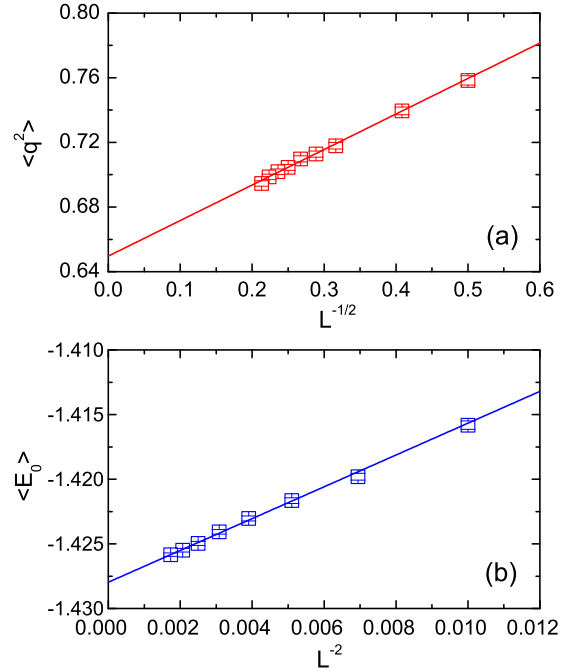

FIG. 7. Equilibrium results (a) $\langle q_{\rm eq}^2(L) \rangle$ and (b) $\langle E_0(L) \rangle$ for $x = 0.5$ and $T \to 0$. We obtain the results $\langle q_{\rm eq}^2(\infty) \rangle = 0.649(4)$ and $\langle E_0(\infty) \rangle = -1.4279(2)$ by extrapolating the data to an infinite size using the form of the size correction.

we consider the model at $x = 0.5$ by using simulated annealing, which allows us to anneal the system to $T = 0$ quickly and obtain the nonequilibrium results.

For nonlinear annealing [49,50], we define

$$T = \upsilon(t_{\rm max} - t)^r, \tag{9}$$

where υ is the annealing velocity. υ can be defined as $\upsilon = (T_{\rm ini} - T_c)/t_{\rm max}^r$, where $t_{\rm max}$ denotes the total MC annealing steps from an initial temperature $T_{\rm ini}$ to the critical temperature T_c, which is zero for the 2D ISG. The critical annealing velocity can be obtained from the KZ mechanism and expressed as $\upsilon_{\rm KZ}(L) \propto L^{-(zr+\Theta_s)}$. The KZ scaling form of a singular quantity can be written by using the annealing velocity and system size when the annealing velocity υ is slower than the critical velocity $\upsilon_{\rm KZ}(L)$:

$$A(\upsilon, L) = L^{-\kappa\Theta_s} F(\upsilon/\upsilon_{KZ}) = L^{-\kappa\Theta_s} F(\upsilon L^{zr+\Theta_s}), \tag{10}$$

where z is the dynamic exponent defined by the relaxation time τ and equilibrium spatial correlation length ξ,

$$\tau \propto \xi^z. \tag{11}$$

We regenerate the distribution of J_2 before each annealing to ensure the correctness of the annealing results. We use a sufficiently high $T_{\rm ini} = 5$ to ensure that the annealing process starts from the paramagnetic state. In accordance with Eq. (9), we perform the annealing from the initial temperature to zero temperature. For accurate results, numerous statistics are necessary; thus, we perform thousands of annealing processes to average the results.

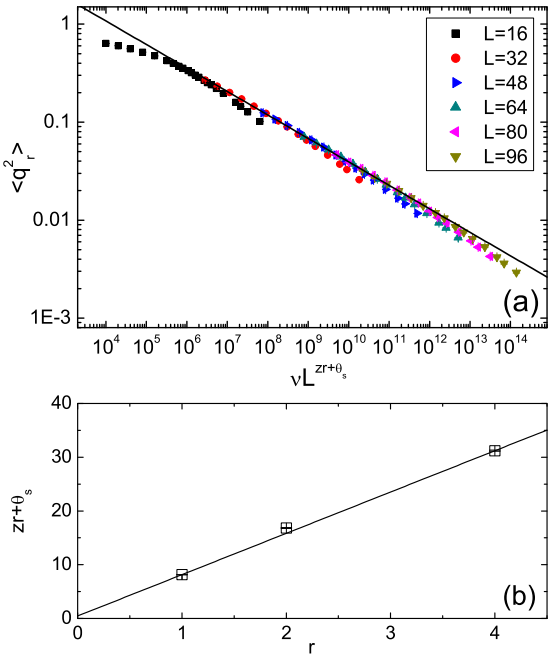

FIG. 8. (a) We can obtain the result of $zr + \Theta_s$ when $r = 1$ by rescaling $\langle q^2 \rangle$ by $\langle q^2 \rangle / \langle q^2_{\rm eq} \rangle$ and fitting the data. (b) reflects the results of $zr + \Theta_s$ vs r. We can obtain $z_q = 7.68(4)$ and $\Theta_s = 0.48(4)$ by annealing with different values of r.

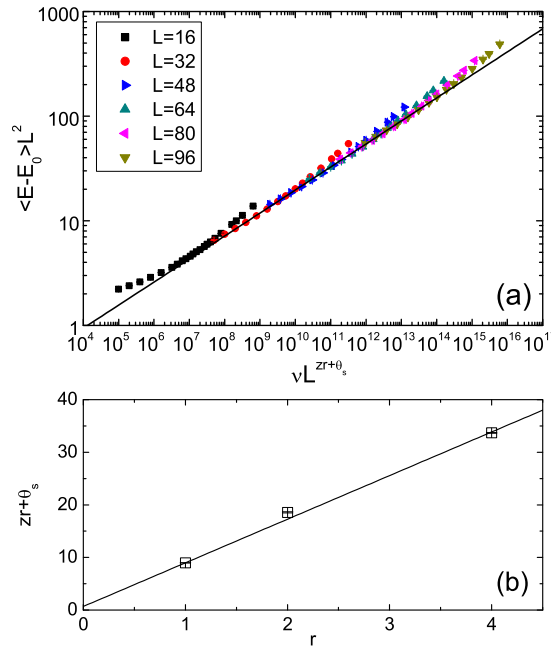

FIG. 9. (a) Mean energy minus the equilibrium ground-state energy of infinite size multiplied by L^2. Here, the results of $r = 1$ are presented. (b) Results of $zr + \Theta_s$ vs r. We perform the same treatment demonstrated in Fig. 8(b), but the results are different: $z_E = 8.44(2)$ and $\Theta_s = 0.51(3)$.

Before fitting the results, we rewrite the KZ scaling form of the EA order parameter as

$$\langle q^2(\upsilon, L) \rangle = \langle q^2_{\rm eq}(L) \rangle F(\upsilon L^{zr+\Theta_s}), \tag{12}$$

where $\langle q^2_{\rm eq}(L) \rangle$ is given by the previous equilibrium finite-size scaling form in Eq. (7). $\langle q^2(\upsilon, L) \rangle \to \langle q^2_{\rm eq}(L) \rangle$ when $\upsilon \to 0$. In Fig. 8(a), we define $\langle q^2_r \rangle = \langle q^2 \rangle / \langle q^2_{\rm eq} \rangle$, and the results can be fitted well on a straight line for $\upsilon < \upsilon_{\rm KZ}(L)$. We obtain the results for z and Θ_s from $zr + \Theta_s$ by setting $r = 1,2,4$, as shown in Fig. 8(b).

The KZ scaling form of the mean energy can be written as

$$\langle E(\upsilon, L) - E_0(\infty) \rangle = L^{-2} F(\upsilon L^{zr+\Theta_s}). \tag{13}$$

Figure 9 illustrates the annealing results of the mean energy, which are analyzed using the same technique presented in Fig. 8.

We obtain two dynamic exponents, z_q and z_E, for the mean energy and EA order parameter, respectively, by checking the finite-size corrections to the scaling form of the EA order parameter and mean energy. Figures 8 and 9 show that the results of different annealing velocities and sizes can be rescaled in accordance with Eqs. (12) and (13), respectively. The results $zr + \Theta_s$ of annealing paths $r = 1,2,4$ are consistent with the entropy exponent obtained from $z_q r + \Theta_s$ and $z_E r + \Theta_s$, thus confirming $\Theta_s \cong 0.5$.

A similar situation is found in the 2D $\pm J$ ISG model described in Ref. [15], where a detailed explanation is provided by using droplet theory. Here, we discuss this atypical situation from the characteristics of spin glass. Spin glass has short-range order and long-range disorder, thereby implying that spin glass has several ordered clusters, whereas the clusters have no correlation with one another. The EA order parameter begins to access the stabilized value when the ordered clusters emerge. Considering the energy landscape of a spin glass, the clusters are ordered in the ground state and the metastable state (local minima). In the annealing process with the slow velocity, the system first enters the metastable state where the value of the EA order parameter begins to stabilize, but the energy continues to change until the system finally reaches the ground state. Therefore, the relaxation time τ is shorter for the EA order parameter than for the energy, and hence, the dynamic exponent z_q is smaller than z_E for the same system (with the same correlation length ξ).

Simultaneously, we perform simulated annealing with $r = 1$ for $x = 0.4$ and 0.65 to obtain the dynamic exponents z_q and z_E. We find that the values of the dynamic exponents are increasing and the difference between z_q and z_E becomes large for $x = 0.4, 0.5, 0.65$. These results show that the energy landscape of the spin-glass phase in our model is not immutable, and its complexity varies with the change in x.

IV. DISCUSSION

The model we study here has a structure similar to the FeAs plane of the iron-based superconducting material $BaFe_2(As_{1-x}P_x)_2$, as detailed in Sec. II A. The superconducting behavior of $BaFe_2(As_{1-x}P_x)_2$ has been studied in previous experiments [24–26]. Our study focuses on the magnetism but still has important implications for real materials. We can obtain a certain interesting coincidence by comparing Fig. 5(a) with the experimental phase diagrams for superconductivity of $BaFe_2(As_{1-x}P_x)_2$ in Refs. [24–26].

The stripe antiferromagnetic phase in Fig. 5(a) ($0 \leqslant x < 0.31$) demonstrates a distribution similar to the phase obtained

from the experiment, which has antiferromagnetic order. Even the critical point of the stripe antiferromagnetic phase $x_c = 0.31(1)$ is similar to that of the experimental results. On the right side of the phase diagram, we obtain a Néel phase for $0.73 < x \leqslant 1$. The Néel phase can possibly suppress the appearance of superconductivity. Our spin-glass phase appears at $0.31 < x < 0.73$, where superconductivity exists but the long-range magnetic order does not exist. The spin-glass phase is a special magnetic phase which does not exhibit global magnetism and long-range order. This character provides an advantageous environment for the emergence of superconductivity. The simultaneous appearance of superconductivity and spin glass was claimed in other superconducting materials [51]. For $BaFe_2(As_{1-x}P_x)_2$, spin-glass-like behavior was suggested by the NMR and TRISP measurements for samples near the optimal region [24].

V. CONCLUSIONS

In this study, we used two MC methods (parallel tempering and simulated annealing) to investigate a bond-diluted J_1-J_2 Ising model by changing the dilution ratio x from 0 to 1. Frustration and disorder were observed in the model. Various thermodynamic quantities were calculated for different values of x through the parallel temperature MC, and an interesting phase diagram was found in which a spin-glass phase exists. In the region $0 \leqslant x < 0.31$, a stripe antiferromagnetic phase is found due to the frustration, and the order of the system is not completely broken. In the region of $0.73 < x \leqslant 1$, the system maintains the Néel order as in $x = 1$ until the dilution ratio reaches the critical point. The spin-glass phase was found in the region $0.31 < x < 0.73$ and was discussed from the equilibrium finite-size scaling where the scaling forms are similar to those of the 2D $\pm J$ ISG model. We performed simulated annealing at the typical value $x = 0.5$, from which we obtained two dynamic exponents, z_q and z_E, of the mean energy and EA order parameter, respectively, by using the KZ mechanism. The determination of two different dynamic exponents from the same annealing process is an atypical phenomenon. Since we have obtained certain results similar to those for the 2D $\pm J$ ISG model, we may connect our model with the 2D $\pm J$ ISG model, which is a classical 2D ISG model, although the distribution of interactions is different.

The magnetism of the iron-based superconducting material $BaFe_2(As_{1-x}P_x)_2$ on Fe can be described by the model that we studied here. In this material, the next-nearest-neighbor interactions J_2 are controlled by the As atoms, which can be substituted by the P atoms. An interesting discovery is that our phase diagram is similar to the experimental phase diagram of $BaFe_2(As_{1-x}P_x)_2$, which helps us understand the magnetism behind the material.

ACKNOWLEDGMENTS

We are sincerely grateful to A. W. Sandvik, E. W. Carlson, W. F. Tsai, E. Dagotto, J. P. Hu, and N. Xu for helpful discussions. This project is supported by NKRDPC-2017YFA0206203, NSFC-11574404, NSFC-11275279, NSFG-2015A030313176, the Special Program for Applied Research on Super Computation of the NSFC-Guangdong Joint Fund, the National Supercomputer Center in Guangzhou, and the Leading Talent Program of Guangdong Special Projects.

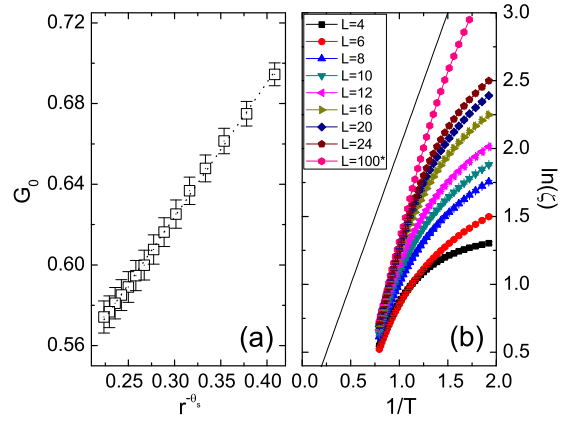

FIG. 10. (a) Behavior of the correlation function G_0 at large r. Here, $x = 0.5$, $L = 48$, $T = 0.00002$. We can obtain a favorable linear fitting by using $\Theta_s = 0.5$; thus, we can consider that $\Theta_s \cong 0.5$ is also established. (b) $\ln(\xi)$ vs $1/T$, reflecting the correlation length that diverges exponentially at $x = 0.5$. We can extrapolate the results for $L = 100$ and deduce that ξ has the form of $\xi \sim \exp(2\beta J)$ when $T \to 0$ and $L \to \infty$. Finally, we can obtain $\nu \to \infty$.

APPENDIX: CONNECTIONS WITH THE 2D $\pm J$ ISG MODEL

The 2D $\pm J$ ISG model is a classical spin-glass model. Section III B 1 states that the properties of the 2D ISG vary in different models. We pay further attention to the scaling form of the 2D $\pm J$ ISG model for other physical quantities because the spin glass here has behavior similar to that of the 2D $\pm J$ ISG model with the EA order parameter.

Thomas *et al.* used droplet theory [52] to discuss the 2D $\pm J$ ISG model in Ref. [47]. These researchers provided a scaling of the correlation function $G(\vec{r})$ at $T \to 0$ by using the entropy exponent Θ_s. The correlation function $G_0(\vec{r}) = [\langle\sigma_{\vec{0}}\sigma_{\vec{r}}\rangle_0^2]$ at large r behaved as

$$G_0(\vec{r}) - G_0(\infty) \sim r^{-\Theta_s}, \tag{A1}$$

where $\Theta_s \cong 0.5$ and r represents the distance between two spins.

We perform the same scaling for $G_0(\vec{r})$, as shown in Fig. 10(a), to determine the value of Θ_s in the spin glass here. From the scaling results, we find that $\Theta_s \cong 0.5$ is applicable here. Thus, in Eq. (7), we use 0.5 as the value of Θ_s when we perform the scaling of $\langle q^2\rangle$.

Correlation length is a commonly used physical quantity in the study of spin glass. The value of the critical exponent ν can be determined by $\xi \sim |T - T_c|^{-\nu}$. In the MC simulations, ξ can be obtained from the susceptibility of the spin glass $\chi_{\rm SG}$,

$$\chi_{\rm SG}(\mathbf{k}) = \frac{1}{N}\sum_{i,j}[\langle\sigma_i\sigma_j\rangle^2]_{\rm av} e^{i\mathbf{k}\cdot(\mathbf{R}_i-\mathbf{R}_j)}, \tag{A2}$$

$$\xi_L = \frac{1}{2\sin(|\mathbf{k}_{\rm min}|/2)}\left[\frac{\chi_{\rm SG}(0)}{\chi_{\rm SG}(\mathbf{k}_{\rm min})} - 1\right]^{1/2}, \tag{A3}$$

where $\mathbf{k}_{\rm min} = (2\pi/L, 0)$.

In the study of the 2D $\pm J$ ISG model, one of the points is $\nu \to \infty$, like in Ref. [53]. We confirm that the correlation length ξ in our study exponentially diverged by performing the same analysis conducted in Ref. [53]; Fig. 10(b) displays the results. Therefore, we also determine the outcome of $\nu \to \infty$ here. This finding is used for the equilibrium finite-size scaling form of the ground-state energy in Eq. (8).

[1] K. Binder and A. P. Young, Rev. Mod. Phys. **58**, 801 (1986).
[2] S. F. Edwards and P. W. Anderson, J. Phys. F **5**, 965 (1975).
[3] D. Sherrington and S. Kirkpatrick, Phys. Rev. Lett. **35**, 1792 (1975).
[4] J. R. L. de Almeida and D. J. Thouless, J. Phys. A **11**, 983 (1978).
[5] V. Cannella and J. A. Mydosh, Phys. Rev. B **6**, 4220 (1972).
[6] J. L. Tholence and R. Tournier, J. Phys. Colloques **35**, C4-229 (1974).
[7] M. Ocio, H. Bouchiat, and P. Monod, J. Phys. Lett. **46**, 647 (1985).
[8] P. Monod, J. J. Prejean, and B. Tissier, J. Appl. Phys. **50**, 7324 (1979).
[9] J. J. Prejean, M. J. Joliclerc, and P. Monod, J. Phys. (Paris) **41**, 427 (1980).
[10] J. Villain, J. Phys. C **10**, 1717 (1977).
[11] N. Jinuntuya and J. Poulter, J. Stat. Mech. (2012) P01010.
[12] D. Perez-Morelo, A. Ramirez-Pastor, and F. Roma, Physica A (Amsterdam, Neth.) **391**, 937 (2012).
[13] F. Parisen Toldin, A. Pelissetto, and E. Vicari, Phys. Rev. E **82**, 021106 (2010).
[14] J. Houdayer and A. K. Hartmann, Phys. Rev. B **70**, 014418 (2004).
[15] S. J. Rubin, N. Xu, and A. W. Sandvik, Phys. Rev. E **95**, 052133 (2017).
[16] D. Zobin, Phys. Rev. B **18**, 2387 (1978).
[17] G. Parisi, F. Ricci-Tersenghi, and J. J. Ruiz-Lorenzo, Phys. Rev. E **60**, 5198 (1999).
[18] R. Kenna and J. J. Ruiz-Lorenzo, Phys. Rev. E **78**, 031134 (2008).
[19] J. J. Alonso and B. Allés, Phys. Rev. B **82**, 064425 (2010).
[20] R. Folk, Y. Holovatch, and T. Yavorskii, Phys. Usp. **46**, 169 (2003).
[21] Y.-T. Kang, W.-F. Tsai, and D.-X. Yao, Phys. Rev. B **95**, 134513 (2017).
[22] S. D. Wilson, Z. Yamani, C. R. Rotundu, B. Freelon, E. Bourret-Courchesne, and R. J. Birgeneau, Phys. Rev. B **79**, 184519 (2009).
[23] S. D. Wilson, C. R. Rotundu, Z. Yamani, P. N. Valdivia, B. Freelon, E. Bourret-Courchesne, and R. J. Birgeneau, Phys. Rev. B **81**, 014501 (2010).
[24] D. Hu, X. Lu, W. Zhang, H. Luo, S. Li, P. Wang, G. Chen, F. Han, S. R. Banjara, A. Sapkota, A. Kreyssig, A. I. Goldman, Z. Yamani, C. Niedermayer, M. Skoulatos, R. Georgii, T. Keller, P. Wang, W. Yu, and P. Dai, Phys. Rev. Lett. **114**, 157002 (2015).
[25] S. Jiang, H. Xing, G. Xuan, C. Wang, Z. Ren, C. Feng, J. Dai, Z. Xu, and G. Cao, J. Phys.: Condens. Matter **21**, 382203 (2009).
[26] Y. Nakai, T. Iye, S. Kitagawa, K. Ishida, H. Ikeda, S. Kasahara, H. Shishido, T. Shibauchi, Y. Matsuda, and T. Terashima, Phys. Rev. Lett. **105**, 107003 (2010).
[27] J. Oitmaa, J. Phys. A **14**, 1159 (1981).
[28] S. Jin, A. Sen, W. Guo, and A. W. Sandvik, Phys. Rev. B **87**, 144406 (2013).
[29] S. Jin, A. Sen, and A. W. Sandvik, Phys. Rev. Lett. **108**, 045702 (2012).
[30] A. I. Guerrero, D. A. Stariolo, and N. G. Almarza, Phys. Rev. E **91**, 052123 (2015).
[31] K. Hukushima and K. Nemoto, J. Phys. Soc. Jpn. **65**, 1604 (1996).
[32] K. Hukushima and Y. Iba, AIP Conf. Proc. **690**, 200 (2003).
[33] S. Kirkpatrick, C. D. Gelatt, and M. P. Vecchi, Science **220**, 671 (1983).
[34] C. J. Geyer, in *Computing Science and Statistics, Proceedings of the 23rd Symposium on the Interface* (Interface Foundation of North America, Fairfax Station, VA, 1991), pp. 156.
[35] R. H. Swendsen and J.-S. Wang, Phys. Rev. Lett. **57**, 2607 (1986).
[36] E. Marinari and G. Parisi, Europhys. Lett. **19**, 451 (1992).
[37] A. P. Lyubartsev, A. A. Martsinovski, S. V. Shevkunov, and P. N. Vorontsov-Velyaminov, J. Chem. Phys. **96**, 1776 (1992).
[38] D. J. Earl and M. W. Deem, Phys. Chem. Chem. Phys. **7**, 3910 (2005).
[39] H. G. Katzgraber, S. Trebst, D. A. Huse, and M. Troyer, J. Stat. Mech. (2006) P03018.
[40] R. M. Liu, W. Z. Zhuo, S. Dong, X. B. Lu, X. S. Gao, M. H. Qin, and J.-M. Liu, Phys. Rev. E **93**, 032114 (2016).
[41] A. G. Nikolaev and S. H. Jacobson, in *Handbook of Metaheuristics*, edited by M. Gendreau and J.-Y. Potvin (Springer, Boston, 2010), pp. 1–39.
[42] L. Ingber, Math. Comput. Modell. **18**, 29 (1993).
[43] W. Wang, J. Machta, and H. G. Katzgraber, Phys. Rev. E **92**, 013303 (2015).
[44] T. W. B. Kibble, J. Phys. A **9**, 1387 (1976).
[45] W. H. Zurek, Nature (London) **317**, 505 (1985).
[46] K. Vollmayr, J. D. Reger, M. Scheucher, and K. Binder, Z. Phys. B **91**, 113 (1993).
[47] C. K. Thomas, D. A. Huse, and A. A. Middleton, Phys. Rev. Lett. **107**, 047203 (2011).
[48] I. A. Campbell, A. K. Hartmann, and H. G. Katzgraber, Phys. Rev. B **70**, 054429 (2004).
[49] C.-W. Liu, A. Polkovnikov, and A. W. Sandvik, Phys. Rev. B **89**, 054307 (2014).
[50] Y. Huang, S. Yin, B. Feng, and F. Zhong, Phys. Rev. B **90**, 134108 (2014).
[51] N. Katayama, S. Ji, D. Louca, S. Lee, M. Fujita, T. J. Sato, J. Wen, Z. Xu, G. Gu, G. Xu, Z. Lin, M. Enoki, S. Chang, K. Yamada, and J. M. Tranquada, J. Phys. Soc. Jpn. **79**, 113702 (2010).
[52] D. S. Fisher and D. A. Huse, Phys. Rev. B **38**, 386 (1988).
[53] H. G. Katzgraber and L. W. Lee, Phys. Rev. B **71**, 134404 (2005).